Inorg. Chem. **2005**, *44*, 6346–6358

Addition of Palladium and Platinum Tri-*tert*-Butylphosphine Groups to Re–Sn and Re–Ge Bonds

Richard D. Adams,*,† Burjor Captain,† Rolfe H. Herber,*,‡ Mikael Johansson,† Israel Nowik,‡ Jack L. Smith, Jr.,† and Mark D. Smith†

Contribution from Department of Chemistry and Biochemistry, University of South Carolina, Columbia, SC 29208, and Racah Institute of Physics, The Hebrew University of Jerusalem, 91904 Jerusalem, Israel

Received June 29, 2005

The reaction of $Re_2(CO)_8[\mu\text{-}\eta^2\text{-}C(H)=C(H)Bu^n](\mu\text{-}H)$ with Ph_3SnH at 68 °C yielded the new compound $Re_2(CO)_8(\mu\text{-}SnPh_2)_2$ (**10**) which contains two $SnPh_2$ ligands bridging two $Re(CO)_4$ groups, joined by an unusually long Re–Re bond. Fenske–Hall molecular orbital calculations indicate that the bonding in the Re_2Sn_2 cluster is dominated by strong Re–Sn interactions and that the Re–Re interactions are weak. The ^{119}Sn Mössbauer spectrum of **10** exhibits a doublet with an isomer shift (IS) of 1.674(12) mm s^{-1} and a quadrupole splitting (QS) of 2.080(12) mm s^{-1} at 90 K,characteristic of Sn(IV) in a SnA_2B_2 environment. The IS is temperature dependent, $-1.99(14) \times 10^{-4}$ mm s^{-1} K^{-1}; the QS is temperature independent. The temperature-dependent properties are consistent with the known Gol'danskii–Kariagin effect. The germanium compound $Re_2(CO)_8(\mu\text{-}GePh_2)_2$ (**11**) was obtained from the reaction of $Re_2(CO)_8[\mu\text{-}\eta^2\text{-}C(H)=C(H)Bu^n](\mu\text{-}H)$ with Ph_3GeH. Compound **11** has a structure similar to that of **10**. The reaction of **10** with $Pd(PBu^t_3)_2$ at 25 °C yielded the bis-$Pd(PBu^t_3)$ adduct, $Re_2(CO)_8(\mu\text{-}SnPh_2)_2[Pd(PBu^t_3)]_2$ (**12**); it has two $Pd(PBu^t_3)$ groups bridging two of the four Re–Sn bonds in **10**. Fenske–Hall molecular orbital calculations show that the $Pd(PBu^t_3)$ groups form three-center two-electron bonds with the neighboring rhenium and tin atoms. The mono- and bis-$Pt(PBu^t_3)$ adducts, $Re_2(CO)_8(\mu\text{-}SnPh_2)_2[Pt(PBu^t_3)]$ (**13**) and $Re_2(CO)_8(\mu\text{-}SnPh_2)_2[Pt(PBu^t_3)]_2$ (**14**), were formed when **10** was treated with $Pt(PBu^t_3)_2$. A mono adduct of **11**, $Re_2(CO)_8(\mu\text{-}GePh_2)_2[Pt(PBu^t_3)]$ (**15**), was obtained similarly from the reaction of **11** with $Pt(PBu^t_3)_2$.

Introduction

Platinum−rhenium bimetallic catalysts have attracted great interest because of their superior properties for the important process known as petroleum reforming.[1] Tin is also widely used to modify the activity of noble metal catalysts,[2] and platinum−tin catalysts have been shown to exhibit superior properties for a variety of processes including petroleum reforming.[3,4] Recent studies have shown that polynuclear metal complexes can be excellent precursors for new polymetallic nanoparticle catalysts.[5]

We have shown that bimetallic cluster complexes containing palladium and platinum can be easily prepared from the

* To whom correspondence should be addressed. E-mail: Adams@mail.chem.sc.edu (R.D.A.); herber@VMS.HUJI.AC.IL (R.H.H.).

† University of South Carolina.

‡ The Hebrew University of Jerusalem.

(1) (a) Xiao, J.; Puddephatt, R. J. *Coord. Chem. Rev.* **1995**, *143*, 457. (b) Augustine, S. M.; Sachtler, W. M. H. *J. Catal.* **1989**, *116*, 184. (c) Nacheff, M. S.; Kraus, L. S.; Ichikawa, M.; Hoffman, B. M.; Butt, J.; Sachtler, W. M. H. *J. Catal.* **1987**, *106*, 263.

(2) (a) Huber, G. W.; Shabaker, J. W.; Dumesic, J. A. *Science* **2003**, *300*, 2075. (b) Holt, M. S.; Wilson, W. L.; Nelson, J. H. *Chem. Rev.* **1989**, *89*, 11. (b) Coupé, J. N.; Jordão, E.; Fraga, M. A.; Mendes, M. J. *Appl. Catal. A* **2000**, *199*, 45. (c) Hermans, S.; Raja, R.; Thomas, J. M.; Johnson, B. F. G.; Sankar, G.; Gleeson, D. *Angew. Chem., Int. Ed.* **2001**, *40*, 1211. (e) Hermans, S.; Johnson, B. F. G. *Chem. Commun.* **2000**, 1955.

(3) (a) Cortright, R. D.; Levin, P. E.; Dumesic, J. A. *Ind. Eng. Chem. Res.* **1998**, *37*, 1717. (b) Cortright, R. D.; Dumesic, J. A. *J. Catal.* **1994**, *148*, 771. (c) Cortright, R. D.; Dumesic, J. A. *J. Catal.* **1995**, *157*, 576. (d) Cortright, R. D.; Dumesic, J. A. *Appl. Catal. A* **1995**, *129*, 101. (e) Vilella, I. M. J.; de Miguel, S. R.; de Lecea, C. S.-M.; Linares-Solano, A.; Scelza, O. A. *Appl. Catal. A* **2005**, *281*, 247. (f) Rodriquez, D.; Sanchez, J.; Arteaga, G. *J. Mol. Catal. A* **2005**, *228*, 309. (g) Llorca, J.; Homs, N.; Leon, J.; Sales, J.; Fierro, J. L. G.; Ramierez de la Piscina, P. *Appl. Catal. A* **1999**, *189*, 77.

(4) (a) Burch, R. *J. Catal.* **1981**, *71*, 348. (b) Burch, R.; Garla, L. C. *J. Catal.* **1981**, *71*, 360. (c) Srinivasan, R.; Davis, B. H. *Platinum Met. Rev.* **1992**, *36*, 151. (d) Fujikawa, T.; Ribeiro, F. H.; Somorjai, G. A. *J. Catal.* **1998**, *178*, 58.

(5) (a) Thomas, J. M.; Johnson, B. F. G.; Raja, R.; Sankar, G.; Midgley, P. A. *Acc. Chem. Res.* **2003,** *36*, 20. (b) Thomas, J. M.; Raja, R.; Johnson, B. F. G.; Hermans, S.; Jones, M. D.; Khimyak, T. *Ind. Eng. Chem. Res.* **2003**, *42*, 1563. (c) Johnson B. F. G. *Top. Catal.* **2003**, *24*, 147. (d) Moreno-Manas, M.; Pleixats, R. *Acc. Chem Res.* **2003**, *36*, 638.

10.1021/ic051077x CCC: $30.25
Published on Web 08/12/2005

reactions of the palladium and platinum bis-tri-*tert*-butylphosphine compounds, M(PBu$^t_3$)$_2$, M = Pd or Pt with preformed metal cluster complexes.[6] For example, the reaction of Pd(PBu$^t_3$)$_2$ with the ruthenium carbonyl cluster complexes $Ru_3(CO)_{12}$ and $Ru_6(CO)_{17}(\mu_6\text{-C})$ yields the adducts $Ru_3(CO)_{12}[Pd(PBu^t_3)]_3$ (**1**) and $Ru_6(CO)_{17}(\mu_6\text{-C})[Pd(PBu^t_3)]_2$ (**2**), respectively.[6a]

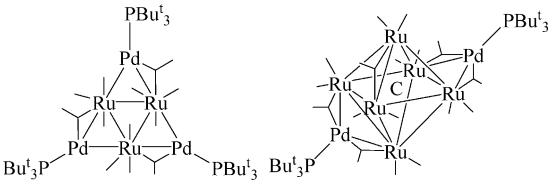

1 **2**

Pd(PBu$^t_3$) and Pt(PBu$^t_3$) groups can exhibit facile dynamical activity. For example, the Pt(PBu$^t_3$) adduct of $Ru_5(CO)_{15}(\mu_5\text{-C})$, $Ru_5(CO)_{15}(\mu_5\text{-C})[PtPBu^t_3)]$ (**3**), exists as both open and closed isomers, **3a** and **3b**, of the metal clusters in solution, and they are in rapid equilibrium on the NMR time scale at room temperature (eq 1).[6b]

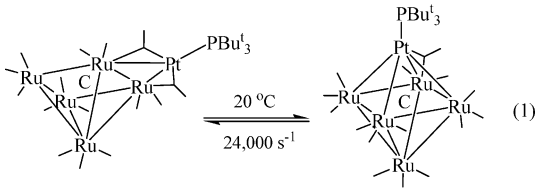

3a **3b** (1)

The bimetallic compounds $Ir_6(CO)_{10}[Pt(PBu^t_3)]_4$ (**4**)[6c] and $Pt_3Re_2(CO)_6(PBu^t_3)_3$ (**5**)[6d] were synthesized from the reactions of Pt(PBu$^t_3$)$_2$ with $Ir_4(CO)_{12}$ and $Re_2(CO)_{10}$, respectively. Both are electronically unsaturated and were found to activate hydrogen under mild conditions.

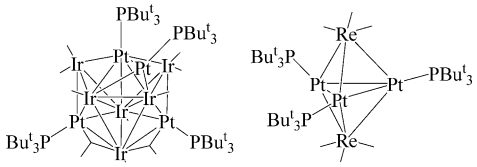

4 **5**

We have also prepared a number of new bimetallic complexes containing tin ligands by the reactions of Ph_3SnH with transition metal carbonyl cluster complexes.[7] This process begins with the oxidative addition of the Sn−H bond to the transition metal clusters and is followed by the cleavage of one or more phenyl groups from the tin atom to form bridging $SnPh_2$ ligands, bridging SnPh ligands, or both. The cleaved phenyl groups combine with the hydrogen atoms and are eliminated as benzene. For example, the complex $Ru_5(CO)_8(C_6H_6)(\mu\text{-}SnPh_2)_4(\mu_5\text{-C})$ (**6**), formed from the reaction of Ph_3SnH with $Ru_5(CO)_{12}(C_6H_6)(\mu_5\text{-C})$, contains four $SnPh_2$ groups that bridge the Ru−Ru bonds along the base of an Ru_5 square pyramid.[7a,b] The addition of Ph_3SnH to rhodium and iridium carbonyl cluster complexes yields products with an even higher tin content. For example, the complex $Rh_3(CO)_3(SnPh_3)_3(\mu\text{-}SnPh_2)_3(\mu_3\text{-}SnPh)_2$ (**7**), formed from the reaction of $Rh_4(CO)_{12}$ and Ph_3SnH, contains eight tin ligands: three terminal $SnPh_3$ groups, three edge-bridging $SnPh_2$ groups, and two triply bridging SnPh groups.[7c] It has also been shown that Ph_3GeH can engage in similar reactions with metal carbonyl clusters to yield products such as $Ru_5(CO)_{11}(\mu\text{-}GePh_2)_4(\mu_5\text{-C})$ (**8**) and $Ir_4H_4(CO)_4(\mu\text{-}GePh_2)_4(\mu_4\text{-GePh})_2$ (**9**), which contain bridging $GePh_2$ ligands.[8] Compound **9** also contains two quadruply bridging GePh ligands.

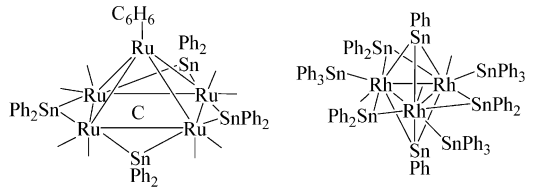

6 **7**

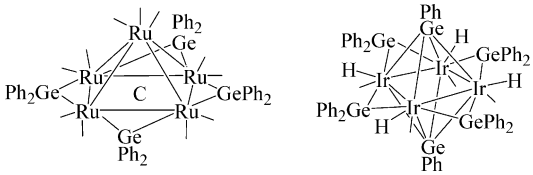

8 **9**

Herein, we demonstrate for the first time that rhenium can be chemically combined both with platinum or palladium and tin to make the first ternary ReSnM complexes, M = Pd or Pt, which could potentially be used as precursors to stoichiometrically precise ReSnM catalysts. A preliminary report on this work has been published.[9]

Experimental Section

General Data. All reactions were performed under a nitrogen atmosphere. Reagent grade solvents were dried by the standard procedures and were freshly distilled prior to use. Infrared spectra were recorded on a Thermo-Nicolet Avatar 360 FT-IR spectrophotometer. ^{1}H NMR spectra were recorded on a Varian Mercury spectrometer operating at 400.1 MHz. ^{31}P{^{1}H} NMR spectra were

(6) (a) Adams, R. D.; Captain, B.; Fu, W.; Hall, M. B.; Manson, J.; Smith, M. D.; Webster, C. E. *J. Am. Chem. Soc.* **2004**, *126*, 5253. (b) Adams, R. D.; Captain, B.; Fu, W.; Pellechia, P. J.; Smith, M. D. *Inorg. Chem.* **2003**, *42*, 2094. (c) Adams, R. D.; Captain, B.; Hall, M. B.; Smith, J. L., Jr.; Webster, C. E. *J. Am. Chem. Soc.* **2005**, *127*, 1007. (d) Adams, R. D.; Captain, B. *Angew. Chem., Int. Ed.* **2005**, *44*, 2531. (e) Adams, R. D.; Captain, B.; Pellechia, P. J.; Smith, J. L., Jr. *Inorg. Chem.* **2004**, *43*, 2695. (f) Adams, R. D.; Captain, B.; Fu, W.; Smith, J. L., Jr.; Smith, M. D. *Organometallics* **2004**, *23*, 589. (g) Adams, R. D.; Captain, B.; Fu, W.; Hall, M. B.; Smith, M. D.; Webster, C. E. *Inorg. Chem.* **2004**, *43*, 3921. (h) Adams, R. D.; Captain, B.; Smith, M. D. *J. Cluster Sci.* **2004**, *15*, 139. (i) Adams, R. D.; Captain, B.; Fu, W.; Smith, M. D. *J. Organomet. Chem.* **2003**, *682*, 113. (j) Adams, R. D.; Captain, B.; Pellechia, P. J.; Zhu, L. *Inorg. Chem.* **2004**, *43*, 7243.

(7) (a) Adams, R. D.; Captain, B.; Fu, W.; Smith, M. D. *Inorg. Chem.* **2002**, *41*, 2302. (b) Adams, R. D.; Captain, B.; Fu, W.; Smith, M. D. *Inorg. Chem.* **2002**, *41*, 5593. (c) Adams, R. D.; Captain, B.; Smith, J. L., Jr.; Hall, M. B.; Beddie, C. L.; Webster, C. E. *Inorg. Chem.* **2004**, *43*, 7576.

(8) (a) Adams, R. D.; Captain, B.; Fu, W. *Inorg. Chem.* **2003**, *42*, 1328. (b) Adams, R. D.; Captain, B.; Smith, J. L., Jr. *Inorg. Chem.* **2005**, *44*, 1413.

(9) Adams, R. D.; Captain, B.; Johansson, M.; Smith, J. L., Jr. *J. Am. Chem. Soc.* **2005**, *127*, 489.

recorded on a Varian Mercury 400 spectrometer operating at 162.0 MHz and were externally referenced against 85% *ortho*-H_3PO_4. Elemental analyses were performed by Desert Analytics (Tucson, AZ). Product separations were performed by TLC in air on Analtech 0.5 mm silica gel 60 Å F_{254} glass plates. $Re_2(CO)_{10}$, $Pd(PBu^t_3)_2$, and $Pt(PBu^t_3)_2$ were obtained from Strem Chemicals, Inc. Ph_3SnH and Ph_3GeH were purchased from Aldrich and were used without further purification. $Re_2(CO)_8[\mu\text{-}\eta^2\text{-}C(H)=C(H)Bu^n](\mu\text{-}H)$ was prepared according to a previously reported procedure.[10]

Synthesis of $Re_2(CO)_8(\mu\text{-}SnPh_2)_2$ (10). Ph_3SnH (200 mg, 0.57 mmol) was dissolved in 5 mL of hexane, and the solution was then added to a solution of $Re_2(CO)_8[\mu\text{-}\eta^2\text{-}C(H)=C(H)Bu^n](\mu\text{-}H)$ (75 mg, 0.11 mmol) in 30 mL of hexane. The reaction mixture was heated to reflux for 2 h. After the mixture was cooled, the solvent was removed in vacuo. The product was separated by TLC using a 3:1 hexane/CH_2Cl_2 solvent mixture to yield 64.8 mg (52% yield) of yellow $Re_2(CO)_8(\mu\text{-}SnPh_2)_2$ (**10**). Spectral data for **10**. IR (cm^{-1} in hexane): ν_{CO} 2060 (m), 2008 (s), 1981 (m), 1972 (m). ^1H NMR (CD_2Cl_2): δ 7.69 (m, 8 H, Ph), 7.43 (m, 12 H, Ph). Anal. Calcd: 33.65, C; 1.76, H. Found: 34.02, C; 2.06, H.

Synthesis of $Re_2(CO)_8(\mu\text{-}GePh_2)_2$ (11). Ph_3GeH (170 mg, 0.57 mmol) was added to a solution of $Re_2(CO)_8[\mu\text{-}\eta^2\text{-}C(H)=C(H)Bu^n](\mu\text{-}H)$ (75 mg, 0.11 mmol) in 30 mL of heptane. The reaction mixture was heated to reflux for 2 h. After the mixture was cooled, the solvent was removed in vacuo, and the product was separated by TLC using a 3:1 hexane/CH_2Cl_2 solvent mixture to yield 37.1 mg (32% yield) of pale yellow $Re_2(CO)_8(\mu\text{-}GePh_2)_2$ (**11**). Spectral data for **11**. IR (cm^{-1} in hexane): ν_{CO} 2068 (m), 2011 (s), 1987 (m), 1982 (m). ^1H NMR (CD_2Cl_2): δ 7.63 (m, 8 H, Ph), 7.40 (m, 12 H, Ph). Anal. Calcd: 36.60, C; 1.92, H. Found: 36.37, C; 2.17, H.

Synthesis of $Re_2(CO)_8(\mu\text{-}SnPh_2)_2[Pd(PBu^t_3)]_2$ (12). $Pd(PBu^t_3)_2$ (56 mg, 0.11 mmol) was added to a solution of **10** (25 mg, 0.022 mmol) in 25 mL of CH_2Cl_2. The reaction mixture was stirred at room temperature for 30 min. The solvent was then removed in vacuo, and the product was separated by TLC using a 2:1 hexane/CH_2Cl_2 solvent mixture to yield 24.9 mg (67%) of orange $Re_2(CO)_8(\mu\text{-}SnPh_2)_2[Pd(PBu^t_3)]_2$ (**12**). Spectral data for **12**. IR (cm^{-1} in hexane): ν_{CO} 2074 (w), 2047 (w), 2035 (w), 1998 (s), 1994 (m), 1980 (s), 1962 (m), 1955 (vs), 1821 (w). ^1H NMR (CD_2Cl_2): δ 7.79 (m, 8 H, Ph), 7.30 (m, 12 H, Ph), 1.24 (d, 54 H, CH_3, $^3J_{P-H}$ = 13 Hz). $^{31}P\{^1H\}$ NMR (CD_2Cl_2): δ 85.4 (s, 2 P). Anal Calcd: 38.22, C; 4.24, H. Found: 37.85, C; 3.93, H.

Synthesis of $Re_2(CO)_8(\mu\text{-}SnPh_2)_2[Pt(PBu^t_3)]$ (13) and $Re_2(CO)_8(\mu\text{-}SnPh_2)_2[Pt(PBu^t_3)]_2$ (14). $Pt(PBu^t_3)_2$ (40 mg, 0.067 mmol) was added to a solution of **10** (25 mg, 0.022 mmol) in 25 mL of hexane. The reaction mixture was heated to reflux for 6 h. The solvent was removed in vacuo, and the products were separated by TLC using a 2:1 hexane/CH_2Cl_2 solvent mixture to yield, in order of elution, 12.8 mg (38% yield) of orange $Re_2(CO)_8(\mu\text{-}SnPh_2)_2[Pt(PBu^t_3)]$ (**13**) and 1.0 mg (2% yield) of red $Re_2(CO)_8(\mu\text{-}SnPh_2)_2[Pt(PBu^t_3)]_2$ (**14**). Spectral data for **13**. IR (cm^{-1} in hexane): ν_{CO} 2075 (w), 2046 (w), 1997 (s), 1980 (m), 1962 (m), 1789 (w). ^1H NMR (CD_2Cl_2): δ 7.76 (m, 8 H, Ph), 7.38 (m, 12 H, Ph), 1.32 (d, 27 H, CH_3, $^3J_{P-H}$ = 13 Hz). $^{31}P\{^1H\}$ NMR (CD_2Cl_2): δ 118.6 (s, 1 P, $^1J_{Pt-P}$ = 5932 Hz). Anal. Calcd: 34.32, C; 3.08, H. Found: 34.67, C; 2.91, H. Spectral data for **14**. IR (cm^{-1} in CH_2Cl_2): ν_{CO} 2047 (vw), 2021 (w), 1974 (s), 1942 (m), 1776 (w). ^1H NMR (CD_2Cl_2): δ 7.79 (m, 8 H, Ph), 7.28 (m, 12 H, Ph), 1.28 (d, 54 H, CH_3, $^3J_{P-H}$ = 13 Hz). $^{31}P\{^1H\}$ NMR (CD_2Cl_2): δ 139.5 (s, 2 P, $^1J_{Pt-P}$ = 6048 Hz). MS: *e/z* 1977 (M + K), 1938 (M^+).

Synthesis of $Re_2(CO)_8(\mu\text{-}GePh_2)_2[Pt(PBu^t_3)]$ (15). $Pt(PBu^t_3)_2$ (75 mg, 0.125 mmol) was added to a solution of **11** (25 mg, 0.024 mmol) in 25 mL of octane. The reaction mixture was heated to reflux for 12 h. After the mixture was cooled, the solvent was removed in vacuo. The product was separated by TLC by using a 2:1 hexane/CH_2Cl_2 solvent mixture to yield 6.2 mg (18% yield) of orange $Re_2(CO)_8(\mu\text{-}GePh_2)_2[Pt(PBu^t_3)]$ (**15**). Spectral data for **15**. IR (cm^{-1} in hexane): ν_{CO} 2081 (w), 2051 (w), 2000 (s), 1984 (m), 1970 (m), 1786 (w). ^1H NMR (CD_2Cl_2): δ 7.77 (m, 8 H, Ph), 7.30 (m, 12 H, Ph), 1.26 (d, 27 H, CH_3, $^3J_{P-H}$ = 13 Hz). $^{31}P\{^1H\}$ NMR (CD_2Cl_2): δ 114.7 (s, 1 P, $^1J_{Pt-P}$ = 5868 Hz). Anal. Calcd: 36.51, C; 3.27, H. Found: 37.20, C; 3.34, H.

Crystallographic Analyses. Yellow crystals of **10** (triclinic form) and **11** suitable for X-ray diffraction analyses were grown by slow evaporation of solutions in hexane/CH_2Cl_2 solvent mixtures at 5 °C. Yellow crystals of **10** (monoclinic form), orange crystals of **12**, **13**, and **15**, and red crystals of **14** were grown from solutions in benzene/octane solvent mixtures at 5 °C. Each data crystal was glued onto the end of a thin glass fiber. X-ray intensity data were measured with a Bruker SMART APEX CCD-based diffractometer using Mo Kα radiation (λ = 0.71073 Å). The raw data frames were integrated with the SAINT+ program[11] using a narrow-frame integration algorithm. Corrections for Lorentz and polarization effects were also applied with SAINT+. An empirical absorption correction based on the multiple measurement of equivalent reflections was applied in each analysis by using the program SADABS. All structures were solved by a combination of direct methods and difference Fourier syntheses and refined by the full-matrix least-squares method on F^2 using the SHELXTL software package.[12] All non-hydrogen atoms in the main residue were refined with anisotropic displacement parameters. All hydrogen atoms were placed in geometrically idealized positions and included as standard riding atoms during the least-squares refinements. Crystal data, data collection parameters, and the results of the analyses are listed in Tables 1−3.

Crystals of **10**, grown from CH_2Cl_2/hexane, crystallized in the triclinic crystal system. The space group $P\bar{1}$ was assumed and confirmed by the successful solution and refinement of the structure. Crystals of **10** grown from benzene/octane crystallized in a monoclinic modification. The systematic absences in the data were consistent with the space groups *C*2/*c* and *Cc*. The former was chosen and confirmed by the successful solution and refinement of the structure.

Compounds **11** and **14** crystallized in the monoclinic crystal system. For **11**, the systematic absences in the data were consistent with the space groups *C*2, *Cm*, and *C*2/*m*. The space group *C*2/*m* was chosen initially and confirmed by the successful solution and refinement of the structure. For **14**, the space group $P2_1/c$ was identified uniquely on the basis of the systematic absences in the intensity data. The crystal of **14** contains two molecules of benzene from the crystallization solvent that cocrystallized with the complex. Both benzene molecules were successfully located and refined with anisotropic displacement parameters. Compounds **12** and **15** crystallized in the triclinic crystal system. In each case, the space group $P\bar{1}$ was assumed and confirmed by the successful solution and refinement of the structure.

The crystal for compound **13** was identified as a nonmerohedral twin composed of two domains related by a 180° rotation around the reciprocal [0 −1 0] axis. The GEMINI[13] program was used to

(10) Nubel, P. O.; Brown, T. L. *J. Am. Chem. Soc.* **1984**, *106*, 644.

(11) *SAINT+*, version 6.2a; Bruker Analytical X-ray Systems, Inc.: Madison, WI, 2001.

(12) Sheldrick, G. M. *SHELXTL*, version 6.1; Bruker Analytical X-ray Systems, Inc.: Madison, WI, 1997.

Table 1. Crystallographic Data for Compound **10**

empirical formula	$Re_2Sn_2O_8C_{32}H_{20}$	$Re_2Sn_2O_8C_{32}H_{20}$	$Re_2Sn_2O_8C_{32}H_{20}$
fw	1142.26	1142.26	1142.26
cryst syst	triclinic	monoclinic	monoclinic
lattice parameters			
a (Å)	9.5962(5)	12.4615(8)	12.7904(6)
b (Å)	12.6495(7)	10.7519(7)	10.8809(5)
c (Å)	14.5038(8)	23.8216(15)	24.0014(12)
α (deg)	104.3420(10)	90	90
β (deg)	90.5590(10)	100.8370(10)	102.2830(10)
γ (deg)	105.3800(10)	90	90
V (Å^3)	1639.25(15)	3134.8(3)	3263.8(3)
space group	$P\bar{1}$	*C*2/*c*	*C*2/*c*
Z	2	4	4
ρ_{calc} (g cm^{-3})	2.314	2.42	2.325
μ(Mo Kα) (mm^{-1})	8.914	9.322	8.954
temp (K)	296(2)	100(2)	296(2)
$2\Theta_{max}$ (deg)	56.56	56.60	56.56
no. of observations	6488	3741	3597
no. of params	397	199	199
GOF[a]	1.019	1.214	1.068
max shift in cycle	0.002	0.001	0.001
residuals:[b] R1, wR2	0.0398, 0.0956	0.0192, 0.0498	0.0211, 0.0536
abs correction	SADABS	SADABS	SADABS
max/min	1.000/0.485	0.155/0.121	0.639/0.143
largest peak (e Å^{-3})	2.484	0.572	0.906

[a] GOF = $[\sum_{hkl} w(|F_o| - |F_c|)^2/(n_{data} - n_{vari})]^{1/2}$. [b] R1 = $\sum_{hkl}(|F_o| - |F_c||)/\sum_{hkl}|F_o|$; wR2 = $[\sum_{hkl} w(|F_o| - |F_c|)^2/\sum_{hkl} wF^2_o]^{1/2}$; $w = 1/\sigma^2(F_o)$.

Table 2. Crystallographic Data for Compounds **11**, **12**, and **14**

	11	**12**	**14**
empirical formula	$Re_2Ge_2O_8C_{32}H_{20}$	$Re_2Sn_2Pd_2P_2O_8C_{56}H_{74}$	$Re_2Pt_2Sn_2P_2O_8C_{56}H_{74}\cdot 2C_6H_6$
fw	1050.06	1759.67	2093.27
cryst syst	monoclinic	triclinic	monoclinic
lattice parameters			
a (Å)	14.0667(11)	10.8119(7)	14.0204(7)
b (Å)	10.6056(8)	12.4429(8)	14.6505(7)
c (Å)	12.0970(10)	12.9946(8)	17.9884(9)
α (deg)	90	80.1170(10)	90
β (deg)	117.3840(10)	68.9880(10)	108.7180(10)
γ (deg)	90	71.9270(10)	90
V (Å^3)	1602.5(2)	1547.85(17)	3499.5(3)
space group	*C*2/*m*	$P\bar{1}$	$P2_1/c$
Z	2	1	2
ρ_{calc} (g cm^{-3})	2.176	1.888	1.987
μ(Mo Kα) (mm^{-1})	9.435	5.357	8.226
temp (K)	296(2)	296(2)	296(2)
$2\Theta_{max}$ (deg)	50.04	50.06	50.06
no. of observations	1410	4901	5434
no. of paramrs	124	334	388
GOF[a]	1.152	1.042	1.048
max shift in cycle	0.001	0.000	0.001
residuals[b]: R1, wR2	0.0254, 0.0593	0.0365, 0.0887	0.0229, 0.0571
abs correction	SADABS	SADABS	SADABS
max/min	0.686/0.490	0.852/0.610	0.518/0.153
largest peak (e Å^{-3})	1.204	1.809	1.226

[a] GOF = $[\sum_{hkl} w(|F_o| - |F_c|)^2/(n_{data} - n_{vari})]^{1/2}$. [b] R1 = $\sum_{hkl}(||F_o| - |F_c||)/\sum_{hkl}|F_o|$; wR2 = $[\sum_{hkl} w(|F_o| - |F_c|)^2/\sum_{hkl} wF^2_o]^{1/2}$; $w = 1/\sigma^2(F_o)$.

determine the orientation matrices for the twin domains. The intensity data were processed with SAINT version 7.00 for multicomponent crystals.[11] In real space, the reflection indices for the two domains are related by the twin law (by rows) [1 0 0/0 −1 0/−0.649 0 −1]. The data were corrected for absorption effects with the TWINABS subroutine in SAINT. An initial structural model was obtained by direct methods using the reflections from the major twin component only. This model was subsequently refined against the twinned data with excellent results (R1 = 0.038), using SHELXTL.[12] All data from both domains were used in the refinement. On the basis of the batch scale factor for the two domains, the data crystal is composed of 76.7% of the major domain and 23.3% of the minor domain. The compound crystallizes in the space group $P2_1/n$, and there is one complete complex in the asymmetric unit. The final difference map extrema are +0.99/−1.12 e$^-$ Å^{-3}, located near the Re(1) atom.

Molecular Orbital Calculations. All molecular orbital calculations reported herein were performed by using the Fenske−Hall method.[14] The calculations were performed utilizing a graphical user interface developed[15] to build inputs and view outputs from stand-alone Fenkse−Hall (version 5.2) and MOPLOT2[16] binary executables. Contracted double-ζ basis sets were used for the Re 5d, Pd 4d, Sn 5p, Ge 4p, P 3p, and C and O 2p atomic orbitals.

(13) *GEMINI*, version 1.02; Bruker Analytical X-ray Systems, Inc.: Madison, WI, 1999.

(14) Hall, M. B.; Fenske, R. F. *Inorg. Chem.* **1972**, *11*, 768.

Table 3. Crystallographic Data for Compounds **13** and **15**[a]

	13	**15**
empirical formula	$Re_2PtSn_2PO_8C_{44}H_{47}$	$Re_2PtGe_2PO_8C_{44}H_{47}$
fw	1539.66	1447.46
cryst syst	monoclinic	triclinic
lattice parameters		
a (Å)	11.5715(5)	11.7436(4)
b (Å)	23.1038(10)	14.5720(5)
c (Å)	17.8097(7)	14.9178(6)
α (deg)	90	105.0460(10)
β (deg)	102.1550(10)	109.3420(10)
γ (deg)	90	94.8710(10)
V (Å^3)	4654.6(3)	2284.91(14)
space group	$P2_1/n$	$P\bar{1}$
Z	4	2
ρ_{calc} (g cm^{-3})	2.197	2.104
μ(Mo Ka) (mm^{-1})	9.318	9.713
temp (K)	100(2)	296(2)
$2\Theta_{max}$ (deg)	50.06	56.61
no. of observations	9569	9535
no. of params	524	532
GOF[a]	1.016	1.027
max shift in cycle	0.001	0.002
residuals[b]: R1, wR2	0.0381, 0.0745	0.0321, 0.0694
abs correction	SADABS	SADABS
max/min	1.000/0.569	0.379/0.248
largest peak (e Å^{-3})	0.992	1.658

[a] GOF = $[\sum_{hkl} w(|F_o| - |F_c|)^2/(n_{data} - n_{vari})]^{1/2}$. [b] R1 = $\sum_{hkl}(||F_o| - |F_c||)/\sum_{hkl}|F_o|$; wR2 = $[\sum_{hkl} w(|F_o| - |F_c|)^2/\sum_{hkl} wF^2_o]^{1/2}$; $w = 1/\sigma^2(F_o)$.

Hydrogen was used in place of both phenyl and *tert*-butyl groups in these calculations. The Fenske−Hall scheme is a nonempirical approximate method that is capable of calculating molecular orbitals for very large transition metal systems and has built-in fragment analysis routines that allow one to assemble transition metal cluster structures from the ligand-containing fragments.

Mössbauer Measurements. A sample of **10**, consisting of yellow crystals as received, was transferred to a plastic sample holder with minimum exposure to the laboratory environment, rapidly cooled to 78 K, loaded into the precooled cryostat, and subjected to Mössbauer spectroscopic (ME) examination as a function of temperature. While such ME spectra yield reliable values for the two pertinent hyperfine interactions, the isomer shift (IS) and the quadrupole splitting (QS), they are not appropriate for the determination of the lattice dynamical properties of the Sn atom because of the large "texture effect" (i.e., the preferential crystal orientation with respect to the optical axis of the ME measurements). The initial data so acquired will be referred to as **10a**. After an initial set of measurements, the large crystals were warmed to room temperature, thoroughly ground to a fine powder, and mixed with boron nitride before being replaced in the sample holder to overcome this limitation. This procedure reduces the texture effect to a minimal value and permits an accurate determination of the vibrational properties of the metal atom (Sn) as a function of temperature, as will be discussed below. The data acquired with this sample will be referred to as **10b**. The remainder of the ME experimental procedure was as described earlier[17] with the addition of the use of a real-time digital output monitoring program, which permitted temperature control to better than ±0.1 K over the time interval of the ME measurements. Spectrometer calibration was effected using an α-Fe absorber at room temperature. All IS values are reported with respect to the centroid of a $BaSnO_3$ absorber spectrum acquired at 296 K. The minimal line widths observed in the ME spectra are on the order of 0.82 mm s^{-1}, and the difference between this value and the theoretical minimum width (0.642 mm s^{-1}) is ascribed to radiation effects in the two year old ^{119m}Sn source, as well as to minor extraneous line broadening because of uncontrolled environmental effects.

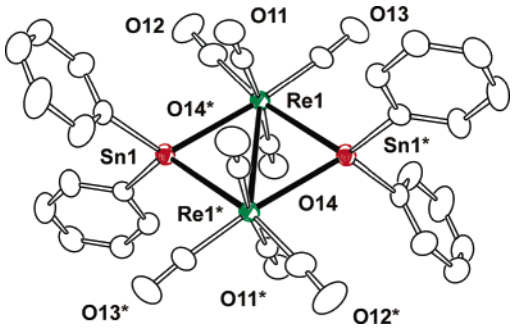

Figure 1. ORTEP diagram of the molecular structure of $Re_2(CO)_8(\mu\text{-}SnPh_2)_2$, **10** (from the triclinic crystalline form), showing 40% thermal ellipsoid probability.

Results and Discussion

Very few examples of rhenium−tin complexes have been reported to date.[18] The new dirhenium-ditin complex $Re_2(CO)_8(\mu\text{-}SnPh_2)_2$ (**10**) was obtained in a 52% yield from the reaction of $Re_2(CO)_8[\mu\text{-}\eta^2\text{-}C(H)=C(H)Bu^n](\mu\text{-}H)$ with an excess of Ph_3SnH at 68 °C. The analogous germanium complex $Re_2(CO)_8(\mu\text{-}GePh_2)_2$ (**11**) was obtained similarly in a 32% yield from the reaction of $Re_2(CO)_8[\mu\text{-}\eta^2\text{-}C(H)=C(H)\text{-}Bu^n](\mu\text{-}H)$ with Ph_3GeH at 97 °C (eq 2).

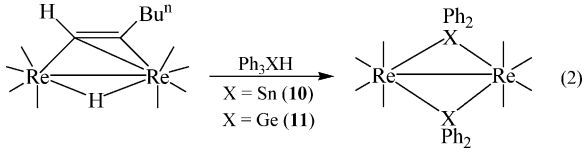

(2)

Both compounds were characterized by a combination of IR, ^{1}H NMR, elemental, and single-crystal X-ray diffraction analyses. Compounds **10** and **11** are isostructural in the solid state, but they are not isomorphous. In fact, compound **10** was obtained in two crystalline modifications: a monoclinic ($C2/c$) and a triclinic ($P\bar{1}$) form (both different from that of **11**). Both forms were investigated by single-crystal X-ray diffraction analyses. Diffraction data for the triclinic form were collected at 296 K, and data for the monoclinic form were collected at both 296 and 100 K. An ORTEP diagram of the molecular structure of **10** (triclinic form) is shown in Figure 1. The molecular structure of **11** is not significantly different. Selected intramolecular distances and angles are listed in Table 4. Both compounds contain two $Re(CO)_4$ groups that are linked by two bridging XPh_2 ligands, X =

(15) Manson, J.; Webster, C. E.; Hall, M. B. *JIMP*, development version 0.1.v117 (built for Windows PC and Redhat Linux); Department of Chemistry, Texas A&M University: College Station, TX; http://www.chem.tamu.edu/jimp/, accessed July 2004.
(16) *MOPLOT2 for orbital and density plots from linear combinations of Slater or Gaussian type orbitals*, version 2.0; Dennis L. Lichtenberger, Department of Chemistry, University of Arizona: Tucson, AZ, 1993.
(17) Nowik, I.; Herber, R. H. *Inorg. Chim. Acta* **2000**, *310*, 191.
(18) (a) Preut, H.; Haupt, H.-J.; Florke, U. *Acta Crystallogr., Sect. C* **1984**, *40*, 600. (b) Haupt, H.-J.; Balsaa, P.; Schwab, B.; Florke, U.; Preut, H. *Z. Anorg. Allg. Chem.* **1984**, *22*, 513. (c) Narayanan, B. A.; Kochi, J. K. *Inorg. Chim. Acta* **1986**, *122*, 85. (d) Westerberg, D. E.; Sutherland, B. E.; Huffman, J. C.; Caulton, K. G. *J. Am. Chem. Soc.* **1988**, *110*, 1642. (e) Huie, B. T.; Kirtley, S. W.; Knobler, C. B.; Kaesz, H. D. *J. Organomet. Chem.* **1981**, *213*, 45.

Table 4. Selected Intermolecular Distances (Å) and Angles (deg) for Compounds **10** and **11**[a]

compound **10**						compound **11**	
P$\bar{1}$ at 296 K		*C*2/*c* at 296 K		*C*2/*c* at 100 K		*C*2/*m* at 296 K	
Re(1)−Re(1)*	3.1971(4)	Re(1)−Re(1)*	3.1685(3)	Re(1)−Re(1)*	3.1542(3)	Re(1)−Re(1)*	3.0510(6)
Re(1)−Sn(1)	2.7429(4)	Re(1)−Sn(1)	2.7567(3)	Re(1)−Sn(1)	2.7491(3)	Re(1)−Ge(1)	2.5923(6)
Re(1)−Sn(1)*	2.7675(5)	Re(1)−Sn(1)*	2.7643(3)	Re(1)−Sn(1)*	2.7682(3)	Re(1)−Ge(1)*	2.5923(6)
C−O (ave)	1.14(1)	C−O (ave)	1.14(1)	C−O (ave)	1.14(1)	C−O (ave)	1.13(1)
Re(1)−Sn(1)−Re(1)*	70.926(11)	Re(1)−Sn(1)−Re(1)*	70.045(7)	Re(1)−Sn(1)−Re(1)*	69.735(7)	Re(1)−Ge(1)−Re(1)*	72.10(2)
Re(1)*−Re(1)−Sn(1)	54.895(10)	Re(1)*−Re(1)−Sn(1)	55.088(6)	Re(1)*−Re(1)−Sn(1)	55.416(6)	Re(1)*−Re(1)−Ge(1)	53.951(11)
Re(1)*−Re(1)−Sn(1)*	54.179(9)	Re(1)*−Re(1)−Sn(1)*	54.866(6)	Re(1)*−Re(1)−Sn(1)*	54.849(5)	Re(1)*−Re(1)−Ge(1)*	53.951(11)
Sn(1)−Re(1)−Sn(1)*	109.074(11)	Sn(1)−Re(1)−Sn(1)*	109.955(7)	Sn(1)−Re(1)−Sn(1)*	110.265(7)	Ge(1)−Re(1)−Ge(1)*	107.90(20)
Re−C−O (ave)	177.2(12)	Re−C−O (ave)	177.2(7)	Re−C−O (ave)	177.3(6)	Re−C−O (ave)	177.1(7)

[a] Estimated standard deviations in the least significant figure are given in parentheses.

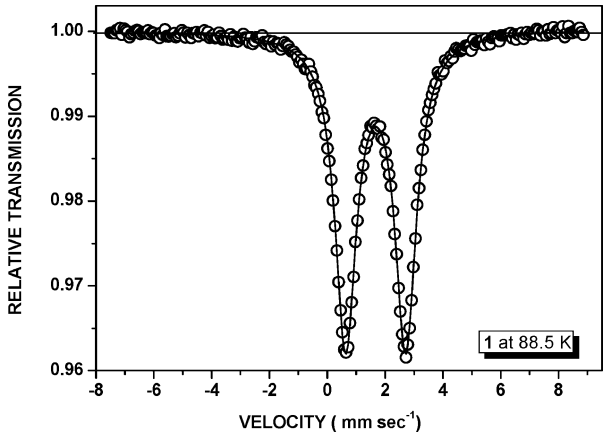

Figure 2. ^{119}Sn Mössbauer spectrum of **10** at 88.5 K. The isomer shift is with reference to a room-temperature $BaSnO_3$ absorber spectrum.

Sn and Ge for **10** and **11**, respectively. According to electron counting procedures, they should both contain a Re−Re single bond so that each rhenium atom can attain the usual 18-electron configuration. The Re−Re distance in **10**, however, is quite long, 3.1685(3) Å, in the monoclinic from at 296 K and is even longer, 3.1971(4) Å, in the triclinic form at 296 K, but it is still short enough to allow for some direct Re−Re interactions and the pairing of the unpaired electron on each $Re(CO)_4$ group, see the molecular orbital calculations below for details. The fact that the Re−Re distance is different by nearly 0.03 Å in the two crystalline modifications at room temperature is consistent with the notion that this bond is not a strong one. The only differences between the molecules in the two crystalline forms of **10** are the weak intermolecular packing forces and the rotational orientations of the phenyl rings on the tin ligands. The Re−Re bond in **11** (3.0510(6) Å) is significantly shorter than that in **10** and only slightly longer than that found for the unbridged Re−Re single bond in $Re_2(CO)_{10}$ (3.042(1) Å).[19]

Mössbauer Spectrum of 10. A typical ^{119}Sn ME spectrum of the finely ground crystalline sample of **10b** at 88.5 K is shown in Figure 2. As expected, the spectrum consists of a simple doublet with well-separated components. The area ratio, $R = A(+)/A(-)$ (where the + and − correspond to the spectrum centroid), of this spectrum is 1.002(4), indicating the high efficacy of the grinding procedure discussed above. The hyperfine parameters and their temperature dependencies are summarized in Table 5. The IS value of 1.674(12) mm s^{-1} at 90 K is consistent with the Sn atom being in the +IV oxidation state, and the QS value of 2.080(12) mm s^{-1} is characteristic of the geometry of the SnA_2B_2 nearest-neighbor environment. A C_2 axis of symmetry passes through the tin atoms and bisects the Re−Re bond. These hyperfine parameters may be compared to those of Ph_2SnCl_2 of similar geometry for which IS is 1.385(27) mm s^{-1} and QS is 2.841(24) mm s^{-1} at 80 K.[20] The temperature dependence of the IS value is summarized graphically in Figure 3 in which the open and full points reflect the data for the crystalline (**10a**) and powder samples (**10b**), respectively. This temperature dependence over the accessible temperature range ($89 < T < 150$ K) is reasonably well fit by a linear regression (slope $= -1.99(14) \times 10^{-4}$ mm s^{-1} K^{-1}, cc = 0.94 for 16 data points) that leads to an effective mass[21] (M_{eff}) of 209(14) Da. The difference between this value and the "bare" Sn atom mass reflects the covalency of the tin−ligand bonding interactions. As will be discussed below, M_{eff} is related to the dynamics of the Sn atom in **10b**.

Table 5. Mössbauer Parameters and Derived Values for **10**

parameter		*T*	units	multiplier
IS (90)	1.674 ± 0.012		mm s^{-1}	
QS (90)	2.080 ± 0.012		mm s^{-1}	
−d*IS*/d*T*	1.99 ± 0.15	88−250 K	mm s^{-1} K^{-1}	10^{-4}
−d ln *A*/d*T*	16.8 ± 1.2	88−250 K	K^{-1}	10^{-3}
Θ_M	47 ± 2		K	
M_{eff}	209 ± 14		Da	
$k^2\langle x^2\rangle$	1.89 ± 0.03	88.5 K		
	2.58 ± 0.05	150 K		
	3.57 ± 0.13	210 K		
	4.29 ± 0.28	250 K		

In contrast, the QS parameter is not a temperature-dependent quantity over the accessible temperature range and all data lie within an error limit of ±0.032 mm s^{-1} of the mean. This temperature independence is readily understood on the basis of the X-ray data at 100 and 296 K, which show that the Re−Sn−Re and C−Sn−C bond angles change by only 1.19 and 2.90 degrees, respectively, over this temperature interval. Similarly, the Re−Sn and Sn−C bond

(19) Churchill, M. R.; Amoh, K. N.; Wasserman, H. J. *Inorg. Chem.* **1981**, *20*, 1609.

(20) (a) Herber, R. H. *J. Inorg. Nucl. Chem.* **1973**, *35*, 67. (b) Debye, N. W. G.; Linzer, M. *J. Chem. Phys.* **1974**, *61*, 4770. (c) Williams, D. E.; Kocher, C. W. *J. Chem. Phys.* **1970**, *52*, 1480. (d) Herber, R. H.; Leahy, M. F. *J. Chem. Phys.* **1977**, *67*, 2718.

(21) Herber, R. H. In *Chemical Mössbauer Spectroscopy;* Herber, R. H., Ed.; Plenum Press: New York, 1984; Chapter VII.

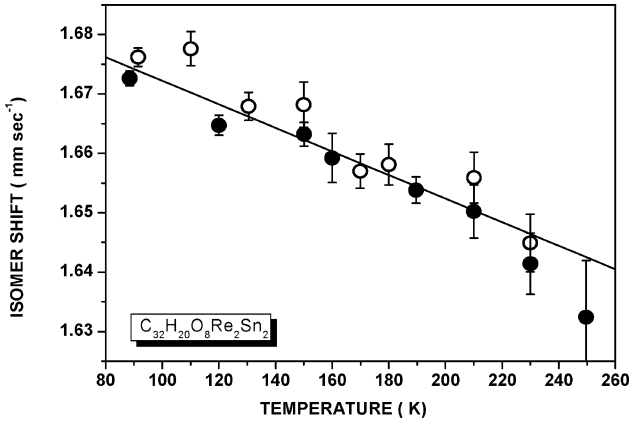

Figure 3. Temperature dependence of the isomer shift of **10**. The open data points refer to the crystalline sample; the closed data points are for the finely ground sample.

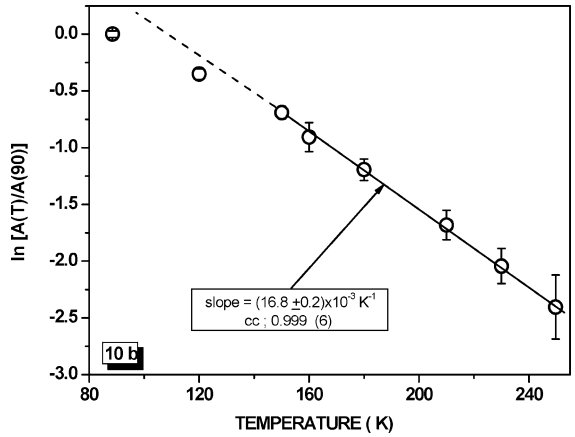

Figure 4. Temperature dependence of the logarithm of the area under the resonance curve (normalized to the 90 K value) for **10b**.

distances change by only 0.0062 and 0.0050 Å, respectively, and these changes are within the error limits of the ME experiments.

The temperature dependence of the area under the resonance curve, which for a thin randomly oriented absorber is identical to the temperature dependence of the recoil-free fraction, *f*, is summarized graphically in Figure 4 for **10b**. The ln *A* data show some curvature, especially at low temperatures. It should be noted that, for a thin absorber, $f = \exp(-k^2\langle x^2\rangle)$ where *k* is the wave vector of the ^{119m}Sn gamma ray and has a numerical value of 1.210×10^9 cm and $\langle x^2\rangle$ is the mean-square amplitude-of-vibration of the Mössbauer active atom. From the high-temperature limiting slope of d ln(*f*/d*T*) and that of the temperature dependence of the IS, it is possible to calculate[21] the effective Mössbauer lattice temperature, Θ_M, and for **10b,** this is found to be to be 47(4) K. This unusually low value for Θ_M is reflected in the limited temperature range over which the ME data could be acquired. In this context, it is appropriate to note that $k^2\langle x^2\rangle$ is also calculable from the $U_{i,j}$ values obtained in a single-crystal X-ray diffraction experiment. For **10b**, these data have been determined at 100 and 296 K (see Supporting Information) and are 1.56 and 5.91, respectively. The low-temperature ME data give $k^2\langle x^2\rangle = 1.7(1)$ at 100 K. Extrapolation of the high-temperature ME data to 296 K

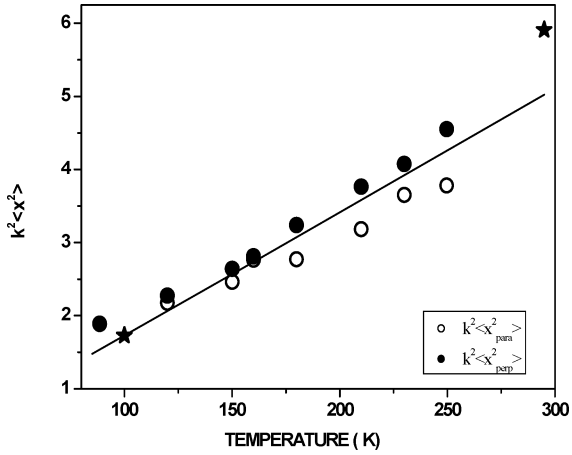

Figure 5. $k^2\langle x^2\rangle$ parameters of **10**. The open data points refer to the values parallel to the C_{2v} axis, while the closed data points pertain to the average perpendicular values. The line corresponds to the $k^2\langle x^2_{ave}\rangle$ for $M_{eff} = 209$ Da and $\Theta_M = 78$ K. The two star symbols are the values calculated from the X-ray crystallographic data at 100 and 296 K.

yields a value of 5.0(3) for this parameter. The satisfactory agreement between these values, keeping in mind the limitation in the temperature range accessible to the ME measurements of such samples, validates the dynamical analysis reported in the present study. In this context, it is worth noting that the IS and QS parameters of **10a** and **10b** are identical (within experimental errors). The area ratio, *R*, which is unity in the low-temperature limit, becomes a temperature-dependent quantity at higher temperatures. This temperature-dependent phenomenon, known as the Gol'danskii−Kariagin effect (GKE),[22] results from the anisotropy of the metal atom motion and has been observed in numerous ^{57}Fe and ^{119}Sn ME spectra. From the magnitudes of *R* and *f* at a given temperature, it is possible to calculate this vibrational anisotropy. The pertinent data for **10b** are summarized in Figure 5. The open data points pertain to $k^2\langle x^2\rangle$ parallel to the 2-fold symmetry axis passing through the metal atom and bisecting the Re−Re bond, while the filled data points reflect the data for the perpendicular values. Moreover, the two parameters are related to $k^2\langle x^2_{ave}\rangle$ by the relationship $k^2\langle x^2_{ave}\rangle = {}^1/_3k^2\langle x^2_{para}\rangle + {}^2/_3k^2\langle x^2_{perp}\rangle$, assuming approximate axial symmetry. Since the ME data at 88.5 K show that $R = 1.002$, the tin atom motion at this temperature must be nearly isotropic, consistent with the 100 K X-ray $U_{i,j}$ values which are 11(1), 13(1), and 8(1) $\times 10^{-19}$ cm^2 respectively, with the off-diagonal elements effectively equal to zero. The $k^2\langle x^2\rangle$ data derived from the ME experiments (which are limited to $T < \sim 260$ K because of the small values of *f* at the higher temperatures) can be fitted separately to a second-order polynomial function, and this procedure yields a value of 4.52 for $k^2\langle x^2_{para}\rangle$ and a value of 5.58 for $k^2\langle x^2_{perp}\rangle$ at 296 K, indicative of a significant vibrational anisotropy of the tin at this temperature. The differences in the root-mean-square

(22) (a) Gol'danskii, V. I.; Makarov, E. F. In *Chemical Applications of Mössbauer Spectroscopy*; Gol'danskii, V. I., Herber, R. H., Eds.; Academic Press: New York, 1968; pp 102−107 and references therein. (b) Herber, R. H.; Nowik, I. *Solid State Sci.* **2002**, *4*, 691. (c) Herber, R. H.; Nowik, I. *Hyperfine Interact.* **2001**, *136*−*137*, 699. (d) Herber, R. H.; Chandra, S. *J. Chem. Phys.* **1971**, *54*, 1847.

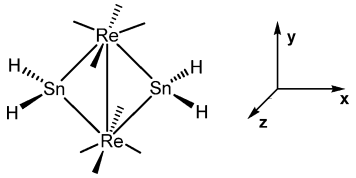

Figure 6. Coordinate system used for the Fenske−Hall molecular orbital calculations.

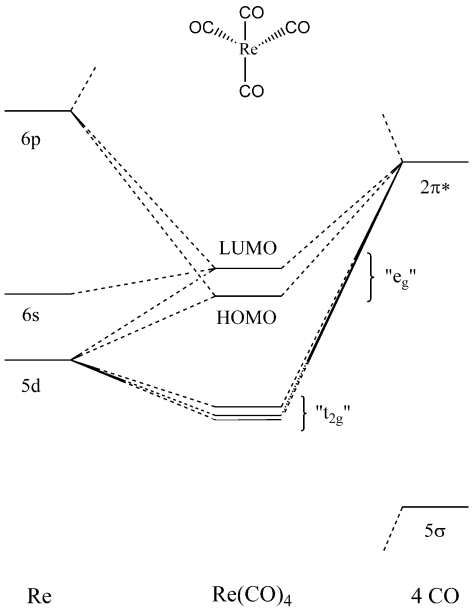

Figure 7. Molecular orbital energy level diagram for the $Re(CO)_4$ fragment.

amplitude-of-vibration of the Sn atom are ∼ 0, 0.057, 0.103, and 0.149 Å at 88.9, 150, 200, and 250 K, respectively.

Molecular Orbital Calculations on Re_2Sn_2 and Re_2Ge_2. We have previously shown that the Rh−Rh and Ir−Ir bonds are unusually long when bridged by a $SnPh_2$ group.[7c] To examine the effect of the two edge-bridging $SnPh_2$ and $GePh_2$ groups on the rhenium−rhenium single bond in **10** and **11**, we performed Fenske−Hall molecular orbital calculations. For these calculations, SnH_2 and GeH_2 groups were used in place of the complete $SnPh_2$ and $GePh_2$ ligands in **10** and **11**, respectively. A schematic of the coordinate system used for these calculations is given in Figure 6. The $Re_2(CO)_8(SnH_2)_2$ cluster was constructed from two $Re(CO)_4$ fragments and two SnH_2 fragments. This model possesses D_{2h} symmetry, and the discussion of its bonding interactions will be based on this symmetry point group. The d^7 $Re(CO)_4$ fragment, which has C_{2v} local symmetry, contains three low-lying filled orbitals derived from the "t_{2g}" set of O_h symmetry and two higher-lying orbitals derived from the "e_g" set which contains one electron, see Figure 7. There is considerable p character in the singly occupied HOMO $d_{x^2-y^2}$ orbital and s and p character in the LUMO d_{z^2} orbital. These metal orbitals interact with the carbonyl $2\pi^*$ (LUMO) orbital.

A linear combination of the two $Re(CO)_4$ fragments in a dinuclear $Re_2(CO)_8$ unit having D_{2h} symmetry is shown in Figure 8. The two sets of three low-lying orbitals are transformed into nondegenerate orbitals of b_{1u}, $1a_g$, and b_{2g} symmetry (which are Re−Re bonding orbitals) and of a_u, b_{3g}, and $1b_{2u}$ symmetry (which are Re−Re antibonding orbitals). These six orbitals are all filled. The two sets of two higher-lying orbitals are transformed into four nondegenerate orbitals of b_{3u}, $2a_g$, b_{1g}, and $2b_{2u}$ symmetry. The HOMO (b_{3u}) and LUMO ($2a_g$) are Re−Re bonding orbitals. The b_{1g} and $2b_{2u}$ are unfilled antibonding orbitals.

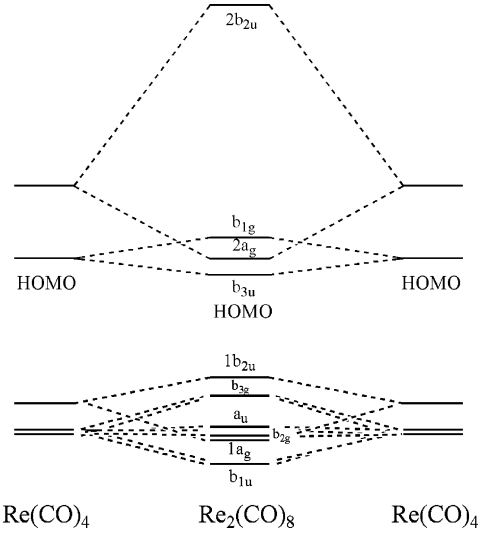

Figure 8. Energy level diagram for the $Re_2(CO)_8$ fragment.

The key orbitals on the SnH_2 fragment are the HOMO "sp^2"-like hybrid orbital and the LUMO p_y orbital that lies perpendicular to the SnH_2 plane. The orbitals for the combined $[SnH_2]_2$ fragment (under D_{2h} symmetry) are derived from the symmetric and antisymmetric combinations of the sp^2-like hybrid orbital (a_g and b_{3u}) and the p_y orbital (b_{2u} and b_{1g}), see right-hand side of Figure 9.

The orbitals of the $Re_2(CO)_8$ fragment combine with orbitals of the $[SnH_2]_2$ fragment of appropriate symmetry and energy to generate the bonding MOs for the $Re_2(CO)_8(SnH_2)_2$ cluster (Figure 9). Favorable interactions of orbitals from the $[SnH_2]_2$ unit lowers the energy of the unoccupied $2a_g$ and b_{1g} orbitals on the $Re_2(CO)_8$ fragment, and these orbitals are then filled by four electrons that are donated by the SnH_2 groups. As was the case with the $Rh_3(CO)_6(SnH_3)_3(\mu\text{-}SnH_2)_3$ model cluster reported in a previous report,[7c] the metal−metal bonding of **10** is dominated by strong Re−Sn interactions. This can be seen in the contour diagrams for the b_{1g} (HOMO), $2a_g$, $1b_{2u}$, $1a_g$, and b_{3u} orbitals shown in Figures 10−12. Significant Re−Re interactions are found only in the $2a_g$ orbital (the HOMO − 2, Figure 11), which explains why the Re−Re distance is unusually long. The b_{3g}, a_u, b_{2g}, and b_{1u} orbitals on the $Re_2(CO)_8$ fragment have no interactions with the orbitals on the $[SnH_2]_2$ fragment.

As noted above, the Re−Re bond distance in **11** is considerably shorter than that in **10**. For comparison, we have also calculated the energies of the Fenske−Hall molecular orbitals of $Re_2(CO)_8(\mu\text{-}GeH_2)_2$ using the positional parameters for **11** for all nonhydrogen atoms. A correlation diagram that compares the energies of the MOs for the $Re_2(CO)_8(\mu\text{-}SnH_2)_2$ and $Re_2(CO)_8(\mu\text{-}GeH_2)_2$ model clusters is shown in Figure 13. For comparison, we will focus on the b_{1g} (HOMO) and the $2a_g$ (HOMO − 2). The b_{3g} (HOMO − 1) has the

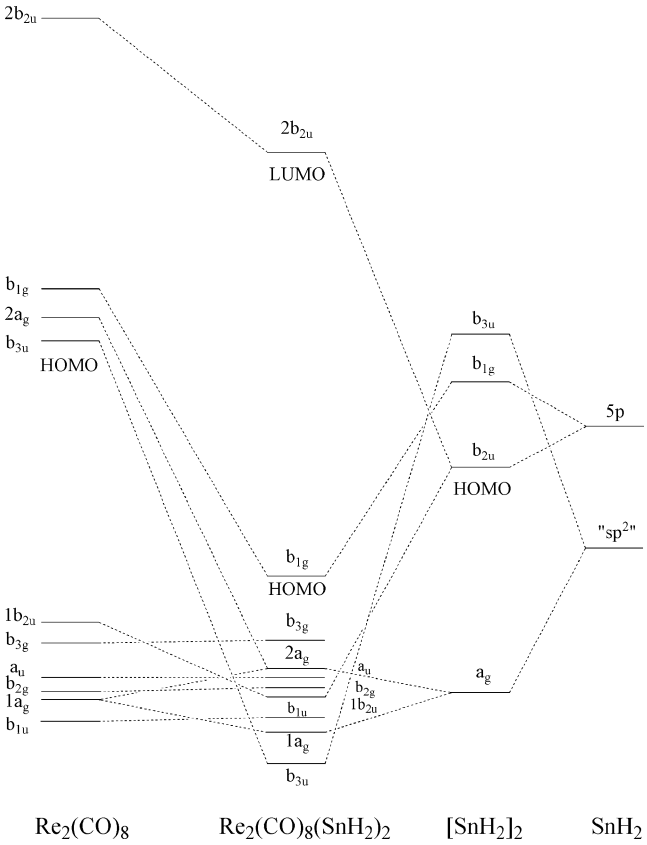

Figure 9. Energy level diagram for the $Re_2(CO)_8(\mu\text{-}SnH_2)_2$ model cluster.

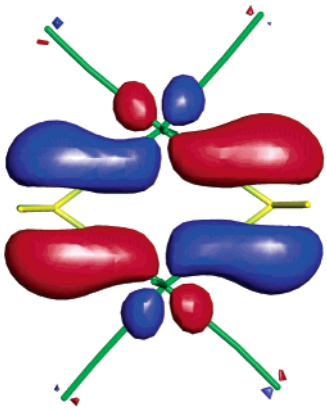

Figure 10. b_{1g} HOMO of the $Re_2(CO)_8(SnH_2)_2$ model cluster showing strong Re−Sn bonding.

same energy in both model compounds. Both the b_{1g} and $2a_g$ orbitals are significantly lower in energy in the $Re_2(CO)_8(\mu\text{-}GeH_2)_2$ model, but most interestingly, we see that the $2a_g$ orbital was lowered by 0.7 eV on going from the Sn compound to the Ge compound, while the b_{1g} orbital was lowered by only 0.6 eV. Because the $2a_g$ orbital is predominantly Re−Re bonding, this would indicate that the Re−Re bond in the Ge form is stronger than that in the Sn form. This is consistent with the observation of a shorter Re−Re bond distance in **11** than in **10**.

Reaction of 10 with $Pd(PBu^t_3)_2$. The importance of the Re−Sn bonding in **10** is further demonstrated by its reaction with $Pd(PBu^t_3)_2$. The reaction of **10** with an excess of $Pd(PBu^t_3)_2$ at 25 °C yielded the complex $Re_2(CO)_8(\mu\text{-}SnPh_2)_2$-$[Pd(PBu^t_3)]_2$ (**12**) in 67% yield. Compound **12** was characterized by a combination of IR, ^1H and $^{31}P\{^1H\}$ NMR, elemental, and single-crystal X-ray diffraction analyses. An ORTEP diagram of the molecular structure of **12** is given in Figure 14. Selected intramolecular distances and angles are listed in Table 6. In the solid state, the compound is crystallographically centrosymmetrical. This compound can be viewed as a bis-$Pd(PBu^t_3)$ adduct of **10** because no ligands were lost from **10** during the course of the reaction. The structure contains two $Pd(PBu^t_3)$ groups that bridge the oppositely positioned Re−Sn bonds of the starting cluster **10**. One carbonyl ligand from each of the original $Re(CO)_4$ groups in **10** has moved into a semi-bridging position on each of the Re−Pd bonds. The Re(1)−Pd(1) bond distance (2.8580(5) Å) is similar in length to one of the two Re−Pd bonds found in the compound $[(\eta^5\text{-}C_4H_4BPh)(CO)_3RePd]_2$ (2.866(1) Å)[23] (the other Re−Pd bond in this compound is much shorter, 2.666(1) Å) but longer than those observed for the compounds $[NEt_4]_2[Re_7(CO)_{21}\{Pd(\eta^3\text{-}PhC_3H_4)\}(C)]$ (2.872(5) Å, average)[24] and $[RePd(CO)_3\{Ph_2P(CH_2)_2PPh_2\}$-$(\eta^5\text{-}7\text{-}CB_{10}H_{11})]$ (2.7858(4) Å).[25] The Pd−Sn bond distance (2.7185(7) Å) is significantly longer than those in the literature (e.g., 2.6082(3) Å as observed for the compound $Pd(PBu^t_2CH_2CH_2PBu^t_2)(\mu\text{-}H)SnMe_3$).[26] The addition of the $Pd(PBu^t_3)$ groups does not significantly alter the length of the palladium bridged Re−Sn bonds (from 2.7675(5) Å in **10** to 2.7674(5) Å in **12**), but curiously, the two Re−Sn bonds not directly associated with the palladium atom, Re(1)−Sn(1)*, have increased in length substantially (from 2.7429(4) Å in **10** to 2.8215(5) Å in **12**). The Re−Re bond distance (3.262(1) Å) is even longer than that found in **10**.

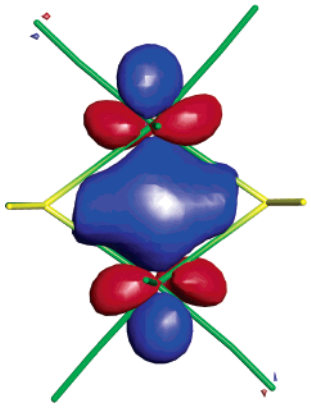

Figure 11. Contour diagram for the $2a_g$ molecular orbital. This orbital contains the only significant Re−Re bonding in the cluster.

Molecular Orbital Calculations on $Re_2Sn_2Pd_2$. The most interesting feature of the bonding of $Pd(PBu^t_3)$ and $Pt(PBu^t_3)$ groups in the adducts, such as **1**, **2**, and **12**, is that the palladium atom is electron deficient and is formally a zero-electron donor.[6a,c,g] In **12,** the palladium−metal bonds that

(23) Braunstein, P.; Englert, U.; Herberich, G. E.; Neuschütz *Angew. Chem., Int. Ed. Engl.* **1995**, *34*, 1010.
(24) Henly, T. J.; Wilson, S. R.; Shapley, J. R. *Inorg. Chem.* **1988**, *27*, 2551.
(25) Blandford, I.; Jeffrey, J. C.; Jelliss, P. A.; Stone, F. G. A. *Organometallics* **1998**, *17*, 1402.
(26) Trebbe, R.; Schager, F.; Goddard, R.; Pörschke, K.-R. *Organometallics* **2000**, *19*, 521.

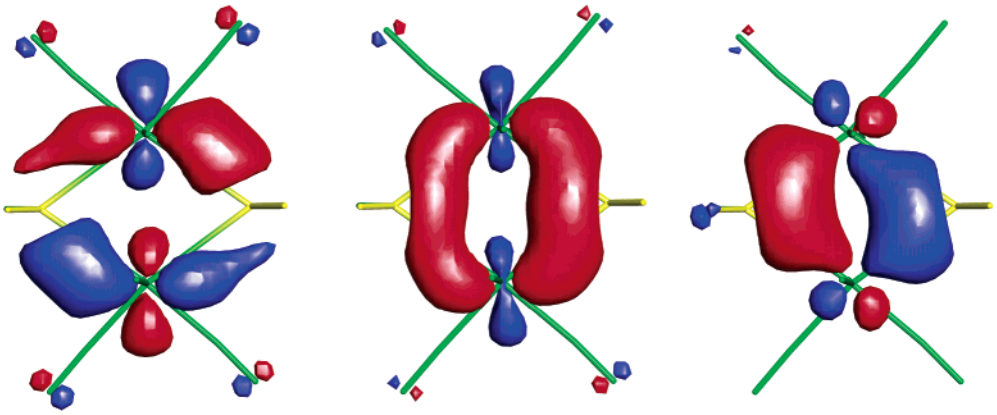

Figure 12. Contour diagrams for the $1b_{2u}$, $1a_g$, and b_{3u} orbitals, respectively, showing Re−Sn bonding.

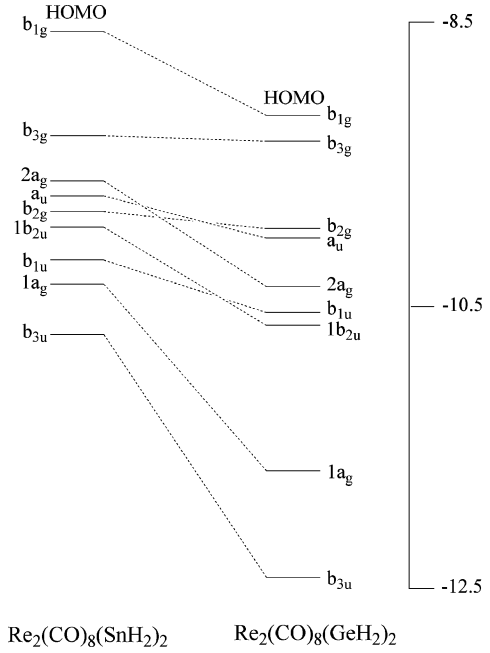

Figure 13. Correlation diagrams for the molecular orbitals of **10** and **11**.

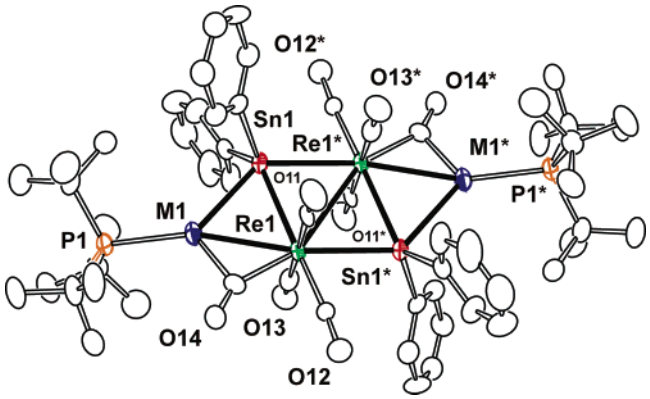

Figure 14. ORTEP diagram of the molecular structure of $Re_2(CO)_8(\mu\text{-}SnPh_2)[M(PBu^t_3)]_2$ (M = Pd for **12** and Pt for **14**) showing 30% thermal ellipsoid probability.

are formed utilize electrons provided by the Re_2Sn_2 cluster, and certain of these bonds are thus delocalized and intrinsically electron deficient. To understand how the bridging palladium phosphine groups bond to the Re_2Sn_2 cluster **12**, we performed Fenske−Hall molecular orbital calculations.

Table 6. Selected Intermolecular Distances (Å) and Angles (deg) for Compounds **12** and **14**[a]

12		**14**	
Re(1)−Re(1)*	3.262(1)	Re(1)−Re(1)*	3.2008(3)
Re(1)−Sn(1)	2.7674(5)	Re(1)−Sn(1)	2.7730(4)
Re(1)−Sn(1)*	2.8215(5)	Re(1)−Sn(1)*	2.8078(3)
Pd(1)−Re(1)	2.8580(5)	Pt(1)−Re(1)	2.7972(2)
Pd(1)−Sn(1)	2.7185(7)	Pt(1)−Sn(1)	2.8166(4)
Pd(1)−P(1)	2.4093(17)	Pt(1)−P(1)	2.3084(12)
C−O (ave)	1.14(2)	C−O (ave)	1.15(1)
Re(1)−Sn(1)−Pd(1)	133.46(2)	Re(1)−Sn(1)−Pt(1)	126.406(12)
Re(1)−Sn(1)−Re(1)*	71.409(13)	Re(1)−Sn(1)−Re(1)*	69.993(9)
Pd(1)−Re(1)−Sn(1)*	164.370(18)	Pt(1)−Re(1)−Sn(1)*	159.520(11)
Sn(1)−Re(1)−Sn(1)*	108.591(13)	Sn(1)−Re(1)−Sn(1)*	110.007(9)
Re−C−O (ave)	175.8(12)	Re−C−O (ave)	176.6(7)

[a] Estimated standard deviations in the least significant figure are given in parentheses.

$Pd(PH_3)$ groups were used instead of the actual $P(Bu^t_3)_3$ groups found in **12**. These groups were added to the MO model developed above for **10**. The key orbitals of the $Pd(PH_3)$ fragment consist of the empty sp_z hybrid orbital and the filled d_{z^2} orbital. An energy level diagram for the resulting $Re_2(CO)_8(\mu\text{-}SnH_2)_2[Pd(PH_3)]_2$ cluster (using approximate C_{2h} symmetry) is shown in Figure 15. Viewed in combination, the two $Pd(PH_3)$ groups form a pair of filled a_g and b_u orbitals from the d_{z^2} orbitals and a similar pair of empty a_g and b_u orbitals from the sp hybrid orbitals. These a_g orbitals interact with the $3a_g$ HOMO (in the C_{2h} symmetry) of the $Re_2(CO)_8(\mu\text{-}SnH_2)_2$ fragment to form the $3a_g$ orbital (HOMO) and the $2a_g$ orbital (HOMO − 2). A contour diagram of the $3a_g$ orbital (Figure 16) shows that the Re−Sn overlap decreases for the bonds *not* directly associated with the palladium, and this is consistent with the observed lengthening of these bonds in **12**. The $2a_g$ orbital (Figure 17), which contains the major direct Re−Re interactions, also contains considerable interactions with the two Pd atoms consisting mainly of the $1a_g$ orbital on the $[Pd(PH_3)]_2$ fragment. The only other molecular orbital of interest is the $2b_u$ orbital (Figure 18), which could be viewed as two three-center interactions between the $Pd(PH_3)$ fragments and the associated Re−Sn bonds. This type of interaction is similar to the one observed previously for the $Ir_4(CO)_{12}[Pt(PH_3)]_2$ model cluster.[6c] Bonding interactions between the palladium and tin atoms in the frontier orbitals are small, which could explain why the Pd−Sn bonds are so long.

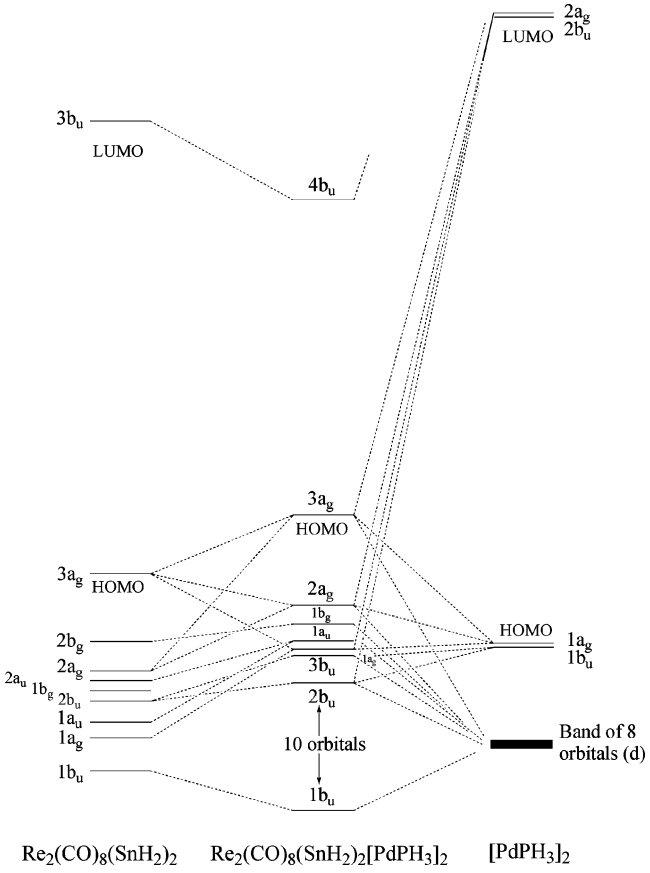

Figure 15. Energy level diagram for the $Re_2(CO)_8(\mu\text{-}SnH_2)_2[Pd(PH_3)]_2$ model cluster.

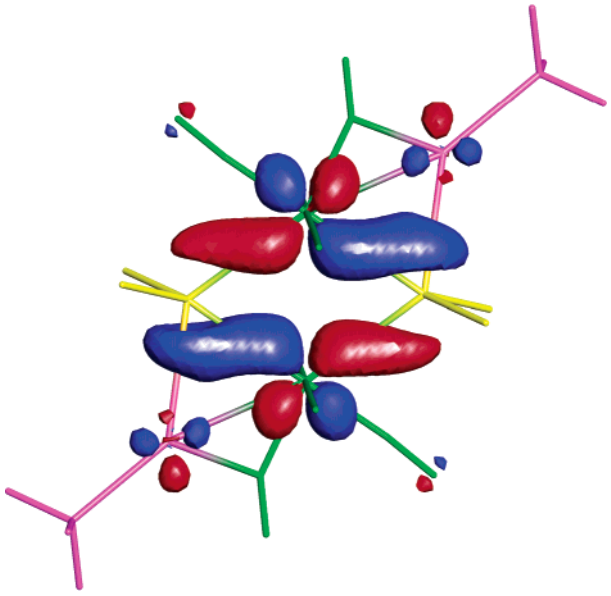

Figure 16. The antibonding $3a_g$ HOMO of the $Re_2(CO)_8(\mu\text{-}SnH_2)_2[Pd(PH_3)]_2$ cluster.

Addition of $Pt(PBu^t_3)$ Groups to 10 and 11. Compound **10** also reacted with $Pt(PBu^t_3)_2$ at 68 °C to yield both the mono- and bis-$Pt(PBu^t_3)$ adducts $Re_2(CO)_8(\mu\text{-}SnPh_2)_2[Pt(PBu^t_3)]$ (**13**) and $Re_2(CO)_8(\mu\text{-}SnPh_2)_2[Pt(PBu^t_3)]_2$ (**14**) in 38 and 2% yields, respectively. Unfortunately, only trace amounts of **14** were obtained and efforts to increase the yield were unsuccessful. Both compounds were characterized by

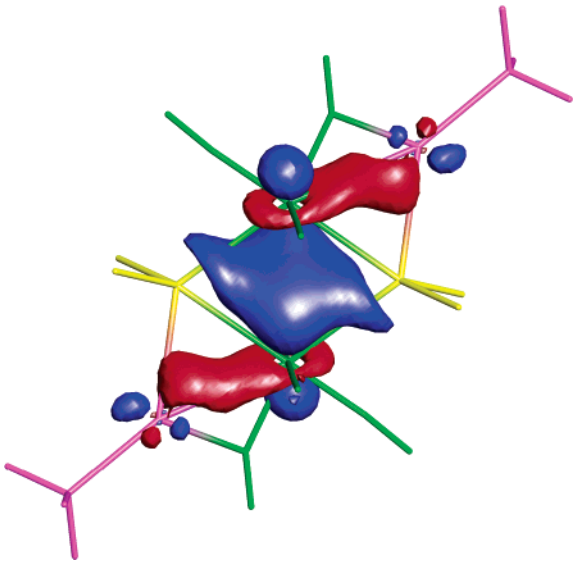

Figure 17. $2a_g$ molecular orbital showing Re−Re and Re−Pd bonding.

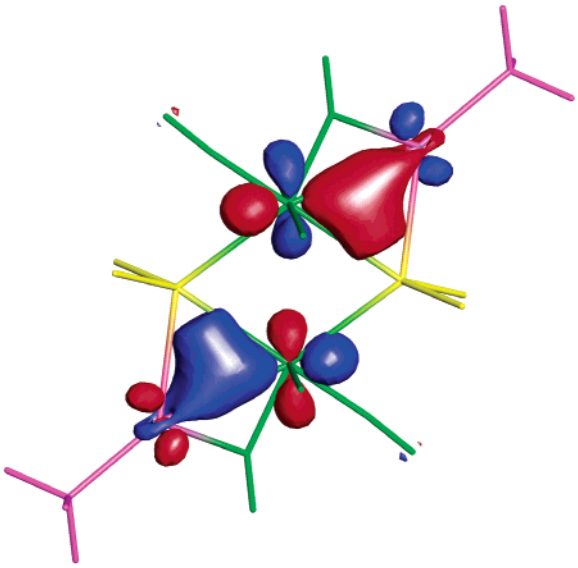

Figure 18. Anti-symmetric $2b_u$ molecular orbital showing the three-center bonding between the $Pd(PH_3)$ groups and the Re−Sn bond.

a combination of IR, ^1H and $^{31}P\{^1H\}$-NMR, and single-crystal X-ray diffraction analyses. An ORTEP diagram of the molecular structure of **13** is given in Figure 19. Selected intramolecular bond distances and angles are listed in Table 7. The structure of **13** consists of a single $Pt(PBu^t_3)$ group that occupies a bridging position on the Re(1)−Sn(1) bond of the starting cluster **10**. A single carbonyl ligand bridges the Re−Pt bond. The Re(1)−Pt(1) bond distance is 2.7932(5) Å is similar in length to the nonhydride bridged Re−Pt bond distances found in $Re_2Pt(CO)_8(PPh_3)_2(\mu\text{-}H)_2$ (2.788(1) Å),[27] $[Re_3Pt(CO)_{14}(\mu\text{-}H)_2]^-$ (2.7778(14) Å and 2.849(2) Å),[28] $Re_2Pt(CO)_8(COD)(\mu\text{-}H)_2$ (COD = 1,5-cyclooctadiene) (2.895(1) and 2.741(1) Å),[29] and $Re_3Pt(CO)_{14}(\mu\text{-}H)_3$ (2.776(1) Å).[29]

(27) Beringhelli, T.; Ceriotti, A.; D'Alfonso, G.; Della Pergola, R. *Organometallics* **1990**, *9*, 1053.
(28) Bergamo, M.; Beringhelli, T.; D'Alfonso, G.; Ciani, G.; Moret, M.; Sironi, A. *Organometallics* **1996**, *15*, 1637.
(29) Antognazza, P.; Beringhelli, T.; D'Alfonso, G.; Minoja, A. *Organometallics* **1992**, *11*, 1777.

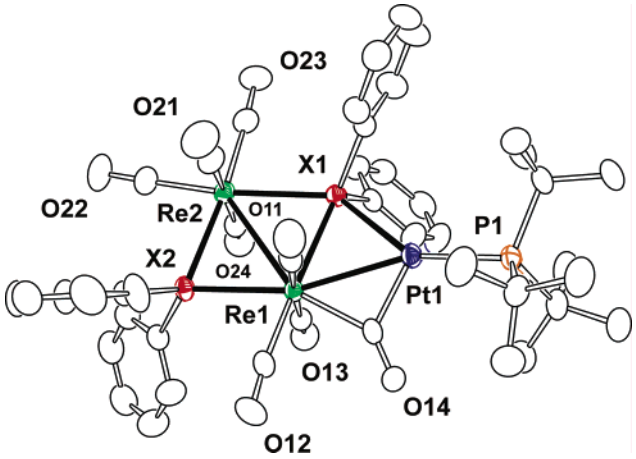

Figure 19. ORTEP diagram of the molecular structures of $Re_2(CO)_8(\mu$-$XPh_2)[Pt(PBu^t_3)]$ (X = Sn for **13** and Ge for **15**) showing 30% thermal ellipsoid probability.

Table 7. Selected Intermolecular Distances (Å) and Angles (deg) for Compounds **13** and **15**[a]

13		**15**	
Re(1)−Re(2)	3.2034(6)	Re(1)−Re(2)	3.0927(3)
Re(1)−Sn(1)	2.8113(8)	Re(1)−Ge(1)	2.6439(5)
Re(1)−Sn(2)	2.7343(8)	Re(1)−Ge(2)	2.5773(5)
Re(2)−Sn(1)	2.8143(8)	Re(2)−Ge(1)	2.6661(5)
Re(2)−Sn(2)	2.7364(9)	Re(2)−Ge(2)	2.5765(5)
Pt(1)−Re(1)	2.7932(5)	Pt(1)−Re(1)	2.8428(3)
Pt(1)−Sn(1)	2.7505(8)	Pt(1)−Ge(1)	2.6324(5)
Pt(1)−P(1)	2.321(2)	Pt(1)−P(1)	2.3337(13)
C−O (ave)	1.14(3)	C−O (ave)	1.15(2)
Re(1)−Re(2)−Sn(1)	55.246(18)	Re(1)−Re(2)−Ge(1)	54.045(12)
Re(1)−Re(2)−Sn(2)	54.126(18)	Re(1)−Re(2)−Ge(2)	53.137(12)
Pt(1)−Re(1)−Re(2)	110.453(17)	Pt(1)−Re(1)−Re(2)	110.643(8)
Pt(1)−Sn(1)−Re(2)	124.78(3)	Pt(1)−Ge(1)−Re(2)	134.33(2)
Pt(1)−Re(1)−Sn(2)	159.22(2)	Pt(1)−Re(1)−Ge(2)	162.714(15)
Re−C−O (ave)	177(1)	Re−C−O (ave)	177(1)

[a] Estimated standard deviations in the least significant figure are given in parentheses.

The Pt(1)−Sn(1) bond distance is 2.7505(8) Å. As in **10**, the Re−Re bond is very long, 3.2034(6) Å. The distances between both rhenium atoms and the platinum-bridged tin atom, Sn(1), are considerably longer, 2.8143(8) Å and 2.8113(8) Å, than the distances between the rhenium atoms and Sn(2), 2.7364(9) Å and 2.7343(8) Å. The latter are slightly shorter than those observed in **10**. The lengthening of the Re−Sn bonds to Sn(1) may be the result of electron delocalization caused by the presence of the bridging Pt-(PBu$^t_3$) group.

Compound **14** is isostructural with **12**, see Figure 14. Selected intramolecular bond distances and angles are listed in Table 6. The lengthening effect observed for the unbridged Re−Sn bonds in **12** is also present in **14** (Re(1)−Sn(1) = 2.8078(3)), however the effect is not as large. The platinum-bridged Re−Sn bonds (2.7730(4) Å) and the Pt−Re bonds (2.7972(2) Å) are all similar in length to those observed in **12**. Unlike the addition of Pd(PBu$^t_3$) to **10**, the addition of the Pt(PBu$^t_3$) groups does not cause a significant increase in the Re−Re bond distance (3.2034(6) Å for **13** and 3.2008-(3) Å for **14**).

Compound **11** also reacted with $Pd(PBu^t_3)_2$ at room temperature, but the products obtained were not sufficiently stable to be isolated and characterized. However, a mono-Pt(PBu$^t_3$) adduct of **11**, $Re_2(CO)_8(\mu$-$GePh_2)_2[Pt(PBu^t_3)]$ (**15**), was obtained in an 18% yield from its reaction with $Pt(PBu^t_3)_2$ at 127 °C. Under these conditions, there was no evidence for the formation of a bis-Pt(PBu$^t_3$) adduct of **11**, and reactions at higher temperatures resulted only in uncharacterizable decomposition products. Compound **15** was characterized by a combination of IR, ^{1}H and ^{31}P{^{1}H}-NMR, elemental, and single-crystal X-ray diffraction analyses. This compound is isostructural with its tin homolog, **13**, see Figure 19. Selected intramolecular bond distances and angles are listed in Table 7. The platinum atom bridges the Re(1)−Ge(1) bond. The Re(1)−Pt(1) bond distance (2.8428(3) Å) is even longer than that in **13**. The Pt(1)−Ge(1) distance of 2.6324(5) Å is significantly longer than that observed for typical Pt−Ge single bonds e.g., Pt−Ge = 2.4495(7) Å in *cis*-$PtMe(GePh_3)(PMe_2Ph)_2$,[30] 2.437(1) Å in $PtEt(GePh_3)(PMe_2$-$Ph)_2$,[31] and 2.4400(4) Å in $PtH(GePh_3)(PPh_3)_2$,[32] indicating that it is very weak. The Re−Re bond distance in **15** (3.0927-(3) Å) is significantly longer than in **11** (3.0510(6) Å). As with **13**, the distances between the rhenium atoms and the platinum-bridged Ge(1) atom have increased significantly in length to 2.6439(5) Å and 2.6661(5) Å, while the distances between the rhenium atoms and Ge(2) are slightly shorter (2.5765(5) Å and 2.5773(5) Å) than those observed in **11** (Re−Ge = 2.5923(6) Å). As with **13**, the increase in all bond distances associated with the platinum atom can be attributed to the delocalization of the electron density in those bonds into the new bonds formed by the associations with the platinum atom. The addition of Pd(PBu$^t_3$) and Pt(PBu$^t_3$) groups to **10** and **11** are summarized in Scheme 1. We were not able to isolate and characterized any mono-Pd(PBu$^t_3$) adducts of **10** or **11**, but in the formation of **12**, a mono adduct must undoubtedly be traversed.

Scheme 1

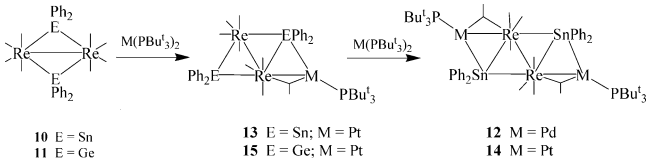

Conclusions

Compounds **10** and **11** further expand the chemistry involving the multiple addition of tin and germanium ligands to metal carbonyl cluster complexes. Compounds **12**−**15** extend the families of complexes with electron deficient metal−metal bonds formed by the addition of M(PBu$^t_3$) (M = Pd, Pt) groups to metal cluster compounds. These compounds represent the first examples of adduct formations between these M(PBu$^t_3$) groups and transition metal−main group metal bonds. Fenske−Hall molecular orbital calculations have been performed to help to understand the unusual

(30) Ozawa, F.; Hikida, T.; Hasebe, K.; Mori, T. *Organometallics* **1998**, *17*, 1018.
(31) Hasebe, K.; Kamite, J.; Mori, T.; Katayama, H.; Ozawa, F. *Organometallics* **2000**, *19*, 2022.
(32) Habereder, T.; Nöth, H. *Appl. Organomet. Chem.* **2003**, *17*, 525.

metal−metal bonding in these complexes. The metal−metal bonding in **10** is dominated by the Re−Sn interactions. The Re−Re interaction is weak, and the Re−Re distance is unusually long. The Pd−Sn, Pt−Sn, and Pt−Ge bonds are also weak. Interestingly, in **12** the unbridged Re−Sn bonds were noticeably weakened when the $Pd(PBu^t_3)$ group was added to the neighboring Re−Sn bond.

Acknowledgment. This research was supported by the Office of Basic Energy Sciences of the U.S. Department of Energy under Grant No. DE-FG02-00ER14980 and the USC Nanocenter. We thank Strem for a donation of a sample of $Pt(PBu^t_3)_2$. The authors thank Drs. M. B. Hall and C. E. Webster for instruction in the use of the Fenske−Hall molecular orbital program package and Prof. W. Glaberson and Dr. Brettschneider for the use of their DASWIN program (available at www.Phys.HUJI.AC.IL/∼glabersn). M.J. thanks the Swedish Research Council for support.

Supporting Information Available: CIF files are available for each of the structural analyses. This material is available free of charge via the Internet at http://pubs.acs.org.

IC051077X